Delft University of Technology

Phosphonate removal from membrane concentrate by electro-coagulation

Serrano, Victor Manuel Torres; Eshun, Lordina Ekua; Farinha, Andreia; Witkamp, Geert Jan; Bucs, Szilard

Citation (APA)
Serrano, V. M. T., Eshun, L. E., Farinha, A., Witkamp, G. J., & Bucs, S. (2022). Phosphonate removal from membrane concentrate by electro-coagulation. *Journal of Environmental Chemical Engineering*, *10*(6), Article 109031. https://doi.org/10.1016/j.jece.2022.109031

Important note
To cite this publication, please use the final published version (if applicable).
Please check the document version above.

Phosphonate removal from membrane concentrate by electro-coagulation

Victor Manuel Torres Serrano [a,b,c,*], Lordina Ekua Eshun [b], Andreia Farinha [a], Geert-Jan Witkamp [a], Szilard Bucs [a]

[a] Water Desalination and Reuse Center (WDRC), Division of Biological and Environmental Science and Engineering (BESE), King Abdullah University of Science and Technology (KAUST), Thuwal 23955–6900, Saudi Arabia
[b] Wetsus, European Centre of Excellence for Sustainable Water Technology, Oostergoweg 9, 8911 MA Leeuwarden, the Netherlands
[c] Department of Biotechnology, Applied Sciences, Delft University of Technology, Building 58, Van der Maasweg 9, 2629 HZ, Delft, the Netherlands

ABSTRACT

In this study, the efficiency of electrocoagulation (EC) with iron electrodes was applied to remove two phosphonates, 1-hydroxyethylidene-1, 1-diphosphonic acid (HEDP) and nitrilotris(methylene) triphosphonic acid (NTMP) from concentrates. This work provides a detailed description of the experimental procedure and results on phosphonate removal and recovery from different electrolytes, including synthetic and real reverse osmosis (RO) membrane concentrates. This research showed high selectivity of EC, removing 100% and 80% of the NTMP and the HEDP respectively, confirming no competition with sulfates, nitrates, or silica. When experimenting with other electrolytes, calcium showed to be critical in enhancing the flocculation process, while calcium carbonate precipitation contributed to capturing the phosphonates from the concentrate. The produced iron oxide (sludge) was confirmed as goethite and akaganéite, and finally transformed into hematite, indicating the oxidation from Fe^{2+} to Fe^{3+} during the EC process. After the iron precipitate collection, an alkaline wash of the sludge was enough to recover 100% of the initial phosphorus from the NTMP phosphonate. However, further research is needed to optimize the recovery procedure and to improve the results with the HEDP. 70 and 140 $A·m^{-2}$ current densities were optimal to bring HEDP and NTMP concentrations down to 32 μM (1 mg·L^{-1}) in only 30 and 10 min respectively. In these conditions, the operational costs, 1.10 and 0.03 €·m^{-3} of treated concentrate, were estimated for HEDP and NTMP respectively. Even when EC has been widely studied for phosphate removal, this technique has been barely applied to treat concentrates containing phosphonate-based antiscalants. EC opens new possibilities for phosphonates and phosphorus to be removed and recovered respectively from membrane and other concentrates.

1. Introduction

Scaling, also known as inorganic or crystalline fouling, occurs when high supersaturation of sparingly soluble salts appears on top of reverse osmosis (RO) membranes [1]. If not treated, scaling negatively affects the operational functioning of the installation by temporally or permanently decreasing permeate quantity and quality. Thus, scaling development makes the process more energy-intensive and costly (operational costs increase 10–15%), requiring cleaning chemicals or the eventual replacement of the membrane [2]. Phosphonates, and other phosphorus compounds, have been proven to delay scaling in membrane filtration processes efficiently [3,4]. Phosphonates are complexing agents that inhibit scaling at low stoichiometric concentrations. Their

high solubility in water and stability at high temperatures make them highly suitable as antiscalants in cooling waters, corrosion inhibitors, additives in cleaning agents, and bleach stabilizers in the textile and paper industry [3,4]. However, the activity of the phosphonates adds complexity to downstream precipitation/softening procedures in RO facilities [5].

Additionally, the presence of (wasted) phosphonates has been reported to have an environmental impact when membrane concentrates are disposed of in surface waters. Recently, researchers claimed that phosphonates had contributed significantly to eutrophication and changes in coral physiology and bacterial behavior in aquatic ecosystems [6,7]. This negative impact of phosphonates on the environment acquires relevance considering the growth of the desalinated water

production between 2016 and 2020, going from 96.5×10^6 m^3·day^{-1} to 114.9×10^6 m^3·day^{-1} [8]. The progressive reduction of the capital expenditures (CAPEX) for RO desalination predicts a continuous expansion in the market for the coming years, particularly in developing countries with pressing water scarcity issues [9]. This also means more significant amounts of membrane concentrates containing phosphonates affecting natural aqueous media. Hence, there is a need to develop a feasible, effective, and efficient approach for phosphonate removal from membrane concentrates.

Iron-based adsorbents have been proposed to remove phosphonates from synthetic and real wastewater [10–17]. Even though adsorption results were satisfactory, this technique involves long contact times and harsh/alkaline conditions for adsorbent regeneration. Chemical coagulation (CC) [18,19] and electrochemical approaches [20–22] have been studied to remove and degrade phosphonates from wastewater. Usually, the CC procedure requires the coagulant concentration to be adjusted depending on the wastewater's pollutant load. Furthermore, chemical coagulation produces a relatively high amount of sludge, which must be appropriately handled, processed, and disposed of as a hazardous material.

EC forces the precipitation/flotation of pollutants by producing the coagulant agent in situ [23]. The coagulant, formed by using an electric current between two electrodes immersed in an electrolyte, destabilizes the electrostatic charge of molecules in suspension, promoting their agglomeration and subsequent precipitation/flotation. Iron and aluminum are the most used coagulants in water treatment and, therefore, the most used materials for electrodes in EC [24]. When using iron, the final products of the reaction are highly insoluble (hydro)oxides and hydroxides, following specific reactions (S1) to (S7) which can be found in the supporting materials [25–27]. The insoluble iron compounds form flocs or sludge (both terminologies will be used indistinctly from now on), providing the active area for the dissolved phosphonates to be adsorbed.

EC has attracted the attention of researchers in recent years due to its high efficiency in reducing the content of chemical oxygen demand (COD) and biological oxygen demand (BOD) [23,25,28–30], TOC [31], nitrates [30,32,33], phosphates [33], arsenic [34], heavy metals [35], or dyes [36] from drinking several types of wastewaters. In addition, EC has several advantages compared to other technologies: (i) it is considered an easy-to-control process; (ii) it reduces the use of chemicals, (iii) it produces less sludge than chemical flocculation/coagulation, (iv) reduced operating costs, and (v) it has the potential of being coupled to renewable energy sources [28,37].

EC has been studied for phosphate removal from concentrates showing good removal results [38,39]. In addition, EC could offer a suitable alternative to adsorption for phosphonate removal from concentrates. Recently, Zhang et al. [40] proved that electrocoagulation (EC) with iron electrodes consumed two-fold less iron than CC to efficiently remove phosphonate-based antiscalants from water. However, they treated a synthetic electrolyte, and their research does not mention the applied current density, nor detailed information about the electrodes. Therefore, it is difficult to compare the study with others and evaluate the efficiency of the process. Apart from Zhang et al., to the best knowledge of the authors, there have been limited detailed studies of phosphonate removal from membrane concentrates using EC. Additionally, this study is augmented by not only EC as the removal technique but for the first time coupled with an estimation of the optimal applied current density and the composition of the precipitated flocs. Furthermore, attempts were addressed for recovering the initial phosphorous from the sludge, opening their potential for being valorized and reused.

For this study two commonly used phosphonates in antiscalant formulations for membrane filtration, 1-hydroxyethylidene-1,1-diphosphonic acid (HEDP) and nitrilotris (methylene) triphosphonic acid (NTMP) [3], were chosen. The first aim of this study is to study the matrix effect on phosphonate removal and iron electrode dissolution

when using synthetic and real membrane concentrates, along with other electrolytes: sodium chloride, calcium chloride, and sodium bicarbonate. It also compares the effect of different current densities in synthetic membrane concentrate. Secondly, the study analyses for the first time the iron precipitate and desorption of phosphorus from flocs and tests the possibility of recovering the phosphorus from these flocs. And lastly, the study concludes with an economic assessment based on the estimated optimal current density.

2. Materials and methods

2.1. Chemicals

All chemicals were reagent-grade and used without further purification unless otherwise specified. The phosphonates HEDP in its monohydrated form, and the NTMP, see Fig. 1, were both acquired from Sigma-Aldrich, The Netherlands. Calcium chloride dihydrate (CaCl$_2$·2 H$_2$O), sodium bicarbonate (NaHCO$_3$), and sodium chloride (NaCl) were supplied by VWR, The Netherlands. The real reverse osmosis concentrate (RROC) was freshly collected from the Engelse Werk water treatment plant (Zwolle, The Netherlands), stored at 4 °C without pretreatment, and used within three days in experiments. All the solutions for experiments were prepared using Milli-Q Billerica demineralized water with TOC < 5 ppb, resistivity no less than 18 MΩ at 25 °C.

2.2. Experimental setup

The electrocoagulation reactor consisted of a 5 L borosilicate beaker covered by a double tailored-made PVC lid that supported the electrodes and sensors. Both lids were connected by 3 PVC screws which gave mobility to the lower one, ensuring the complete immersion of the iron cathode and anode at any time. The anode and the cathode consisted of two ARMCO iron (certified 99.9% purity) round plates supplied by AK Steel, The Netherlands. The electrodes were equal in dimension, 30 mm diameter, 2 mm thickness, and placed 2 cm apart. The two ARMCO iron electrodes were connected to the power supply, through a platinum wire, model ES015–10 Programmable DC 0–15 V 0–10 A from Delta Elektronika, The Netherlands. The pH in the electrochemical reactor was measured using an Orbisint CPS11D pH electrode, Endress and Hauser, The Netherlands, which was calibrated before starting each experiment. The pH data were recorded and saved in a Liquiline CM442 transmitter, Endress and Hauser, The Netherlands. The reactor (cell) was placed on a magnetic Heidolph MR Standard Magnetic Stirrer/Hot Plate at a spinning rate of 120 rpm to ensure the homogeneity of the solution. Fig. 2 schematically depicts the complete experimental setup.

2.3. Experimental procedure

All the experiments were conducted by treating 4 L of electrolyte solution at room temperature and in batch mode. The resulting pH from the preparation of each solution was not modified during the experiments. To maintain a constant total volume of the treated concentrate, 5 mL samples were taken during both 1- and 2-hour experiments. Thus, the variation of the treated concentrate total volume was less than 5% in
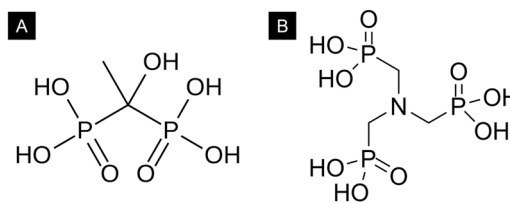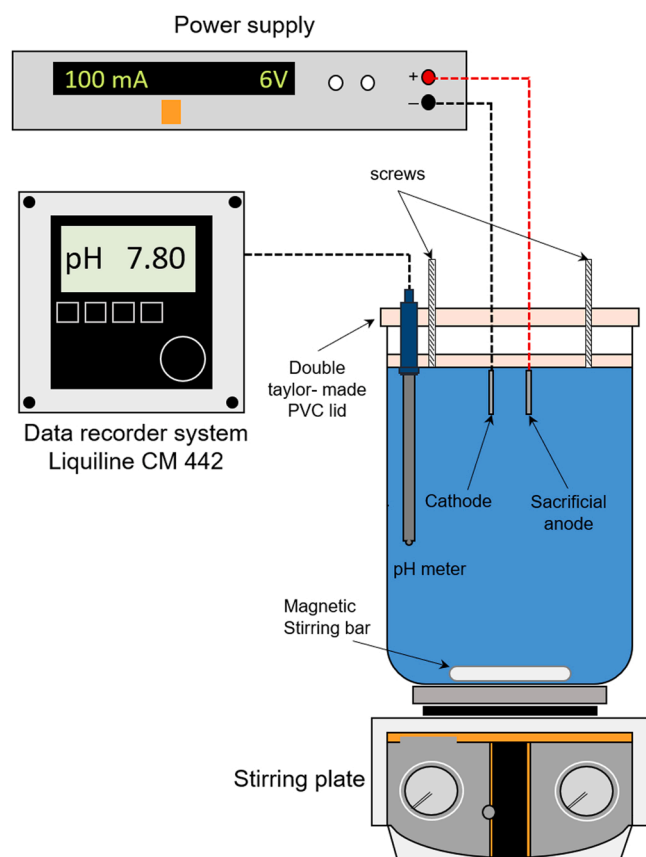

Fig. 1. : Molecular structures of the phosphonates (A) 1-hydroxyethylidene-1,1-diphosphonic acid (HEDP), and (B) Aminotris (methylenephosphonic acid) (NTMP or ATMP).

Fig. 2. : Electro-coagulation experimental set-up for batch experiments with iron electrodes.

both experiments (1.5%, 1 h and 3% 2 h respectively). The samples were subsequently filtered using Millipore 0.22 μm mixed cellulose esters membrane filters, stabilized with 1.5 mL of HNO_3 4% ca., and stored at 4 °C for a maximum of 24 h before the elemental analysis. Liquid samples of 6.5 mL volume were then analyzed for the total iron and phosphorus concentrations using inductively coupled plasma optical emission spectroscopy (ICP-OES) (Optima 5300DV, Perkin–Elmer). The temperature of membrane concentrates does not deviate from 25 °C, (optimal working temperature for RO membranes). Hence, 25 °C was selected as the standard working temperature for all subsequent experiments.

2.3.1. Effect of the electrolyte

The effect of different electrolytes, NaCl, $CaCl_2$, $NaHCO_3$, RROC, and synthetic reverse osmosis concentrate (SROC), was studied on the iron concentration and the phosphorus removal during the EC process. 70 A·m^{-2} current density was used and taken as a reference since it gave one of the best operational conditions for HEDP and NTMP removal (see Section 3.5). The SROC was prepared by mixing two 2 L solutions, one containing either one of the phosphonates and dissolved $NaHCO_3$, and the other one only dissolved $CaCl_2$. The final concentrations (4 L total volume) were 14 mM $NaHCO_3$ and 9 mM $CaCl_2$. The rest of the electrolytes were prepared by keeping the ionic strength, IS, at 41 mM, the same as the SROC. All the solutions, including the RROC, were spiked with the acquired phosphonates to have a 100 μM total phosphorus concentration at the beginning of the experiments. The concentration of dissolved phosphorus was found negligible in the RROC within the detection range of the ICP-OES. Therefore, it was spiked with the phosphonate solution, as described for the SROC. Therefore, it will be assumed that the phosphorus concentrations presented in the corresponding section will be due to the contribution of the phosphonates only. Table 1 summarizes the composition of all the prepared electrolytes.

To estimate the stability of the RROC and SROC regarding the precipitation of different species, the corresponding saturation indexes, SI [dimensionless], for both concentrates were computed by Eq. (1) [41]. IAP is the ionic activity product for each ionic species in solution, and K_{SP} is their respective thermodynamic solubility constant.

$$SI = \log \frac{IAP}{K_{SP}} \tag{1}$$

The Eq. (1) was implemented in the speciation software PHREEQC v3.5.1 (2017) [42], models: Wateq4f and Pitzer for both concentrates RROC and SROC, and the results are shown in Table S1 and Table S2, respectively in the supporting materials. The results obtained for the RROC revealed a SI far below 1 for $CaSO_4$, CaF_2, $BaSO_4$, $SrSO_4$, and iron carbonates. However, it showed supersaturation indexes slightly higher than 1 for calcium carbonate, $CaCO_3$ (calcite and aragonite), and calcium and magnesium carbonates (antigorite, dolomite, huntite, and talc). In the case of the SROC, only calcite and aragonite obtained SI slightly higher than 1. Therefore, RROC and SROC consisted of metastable solutions where the eventual spontaneous precipitation of calcium carbonates and calcium-magnesium carbonates precipitation may occur.

Table 1
Composition of the different electrolytes at fixed 70 A·m^{-2} current density experiments.

Parameter	Units	Electrolyte				
		Real RO membrane concentrate (RROC)	Synthetic membrane concentrate (SROC)	NaCl	$CaCl_2$	$NaHCO_3$
Ca^{2+}	[mM]	9.9	9	–	13.7	–
Mg^{2+}	[mM]	2.4	–	–	–	–
Na^+	[mM]	12.1	14	41	–	41
K^+	[mM]	0.7	–	–	–	–
NH_4^+	[mM]	0.0	–	–	–	–
Ba^{2+}	[mM]	0.0	–	–	–	–
Sr^{2+}	[mM]	0.0	–	–	–	–
CO_3^{2-}	[mM]	0.0	–	–	–	–
HCO_3^-	[mM]	14.8	14	–	–	41
SO_4^{2-}	[mM]	3.1	–	–	–	–
Cl^-	[mM]	13.4	18	41	27.3	–
F^-	[mM]	0.0	–	–	–	–
NO_3^-	[mM]	0.4	–	–	–	–
SiO_3	[mM]	0.6	–	–	–	–
IS (model: Pitzer)	[mM]	51.55	41.27	41.00	41.00	41.00
TDS	[mg·L^{-1}]	2504.9	–	–	–	–
pH	[-]	7.86	7.82	4.77 with HEDP 5.87 with NTMP	4.20 with HEDP 4.28 with NTMP	8.2

2.3.2. Experiments at different current densities

Blank experiments with agitation and without current were performed to observe the extent of the spontaneous electrode oxidation and the phosphorus removal. Subsequently, EC experiments at different current densities, 7, 35, 52, 70, and 140 $A \cdot m^{-2}$ (applied currents: 10, 50, 75, 100, and 200 mA) were carried out also with agitation for 1 and 2 h. Samples were taken every 5 min for iron and phosphorus concentration analysis. All the experiments were performed with the SROC only since the iron dissolution and phosphorus removal turned out to be similar for RROC and SROC.

Typically, current densities between 10 and 100 $A \cdot m^{-2}$, [39,43–46] and exceptionally, up to 400 $A \cdot m^{-2}$ [33] are applied for phosphate removal with EC using aluminum and iron electrodes. Most experiments are performed with several plate electrodes placed in parallel. This electrode layout allows the reactor to operate at low current densities. However, in this study, the electrode area is relatively small which leads to higher applied current densities. Preliminary experiments confirmed that a minimum current of 10 mA (7 $A \cdot m^{-2}$) was required, and subsequent well-spaced currents (e.g., 10, 50, 75, 100, and 200 mA), to obtain the desired phosphonate removal rates in the shortest times and at optimal operational point (see Section 3.5).

2.3.3. Sludge characterization

The sludge produced with synthetic concentrate (70 $A \cdot m^{-2}$) was collected and dried at 60 °C in a vacuum oven for a week. The surface appearance and the elemental composition of the dried sludge were both characterized by Raman spectroscopy (WITec Apyron), Scanning Electron Microscopy (SEM), and Energy Dispersive X-Ray Spectroscopy (EDS or EDX) (JEOL JSM-6480 LV). Table 2 summarizes all the experiments carried out during this research.

3. Results and discussion

The following subsections present the results from the experimental work on phosphonate removal by electrocoagulation. The effects of the electrolyte composition and the current density on the anode dissolution and phosphonate removal are discussed. Then, the characterization of the sludge and the attempts to recover the phosphorus from it are presented. Finally, the study concludes with an economic evaluation of electrocoagulation for phosphonate removal.

3.1. The influence of the electrolyte

Experiments with different electrolytes were performed to evaluate the effectiveness of EC for phosphonate removal. Since this technique has a practical application, we started the experimental set with the RROC and the SROC. First, the blank experiment was performed by introducing the iron electrodes in SROC, containing either HEDP or NTMP, and the reaction was followed by tracking the iron and phosphorus concentrations for one hour. No current was applied during this time. The results revealed spontaneous dissolution of the iron electrodes due to the high concentration of chloride ions in the solution (Fig. 3A). The phenomenon was more remarkable for the HEDP. The phosphorus concentration remained constant when HEDP was present (Fig. 3B). At the same time, it decreased by 20% within the first thirty minutes of the experiment and stayed stable for one hour. Fang et al. [47] reported better anti-corrosion properties of NTMP than HEDP. Their research claimed NTMP formed a passivation layer that efficiently avoided steel corrosion in an oxidant solution for 20 min. The passivation layer formed via a coordination reaction with Fe^{2+}, leading to a $[Fe(NTMP)_2]^0$ coordinated compound. The better anticorrosion properties of the NTMP explain the slower dissolution of the anode compared to the solution containing the HEDP. Therefore, the 20% decrease in phosphorus concentration (Fig. 3B) is mainly due to the formation of the passivation layer on the electrode's surface. As well as to a lesser extent, the potential adsorption on the formed flocs.

Similar iron and phosphorus concentration profiles were obtained using the EC technique with the two concentrates, RROC and SROC, at 70 $A \cdot m^{-2}$ current density. The dissolution of the anode leads to a rapid increase in the iron concentration until it reaches a maximum (Fig. 4A and Fig. 4B). After that point, it subsequently decreases due to a fast formation of the iron oxide flocs and the progressive passivation of the anode [48]. Finally, at the last stages of the experiment, the iron concentration decrease becomes less steep, which suggests similar rates of anode dissolution and iron oxide precipitation. Higher residual iron concentration was found in the case of the RROC, which was due to the composition of the commercial antiscalant used in the desalination plant. Its formulation includes complexing agents to delay the precipitation of iron carbonates. These compounds avoided iron from precipitating as oxides/hydroxides and remained in the solution during the rest of the experiment.

Table 2
Summary of the experimental work performed in this research.

| Experiment	Electrolyte	Current density [$A \cdot m^{-2}$]	Phosphonate	Experimental time [min]	Agitation [rpm]	Sludge surface analysis
Blank	SROC	–	HEDP	60	120	
			NTMP	60	120	
	SROC	70	HEDP	60	–	
			NTMP	60		
1	RROC	70	HEDP	60	120	
			NTMP	60	120	
2	SROC	7	HEDP	60	120	Yes
		35	NTMP	60	120	Yes
		52	HEDP	60	120	
		70	NTMP	60	120	
		140	HEDP	60	120	
			NTMP	60	120	
			HEDP	120	120	
			NTMP	120	120	
			HEDP	60	120	
			NTMP	60	120	
3	NaCl	70	HEDP	60	120	
			NTMP	60	120	
4	CaCl$_2$	70	HEDP	60	120	
			NTMP	60	120	
5	NaHCO$_3$	70	HEDP	60	120	
			NTMP	60	120	
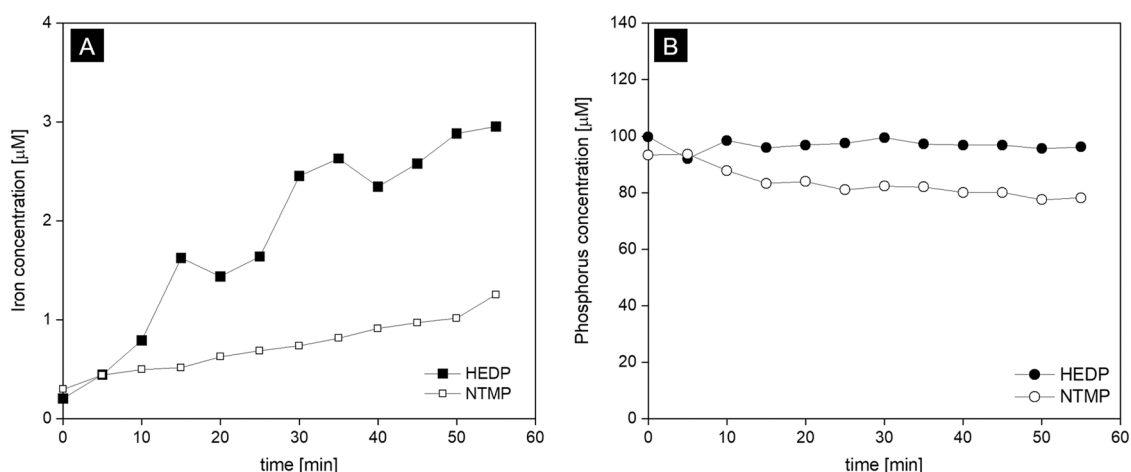
Fig. 3. : Blank experiments exposed the ARMCO iron electrodes to the SROC without applying any current. (A) The iron concentration profiles revealed that there is spontaneous dissolution due to the high concentration of chloride. The dissolution phenomenon is more remarkable in the presence of HEDP phosphonate than with NTMP. (B) The phosphorus removal was almost negligible for HEDP, while it decreased by 20% for NTMP. $CaCl_2$ concentration: 9 mM, $NaHCO_3$ concentration: 14 mM. Initial phosphorus concentration: 100 µM, IS: 41.27 mM, initial pH: 7.82.
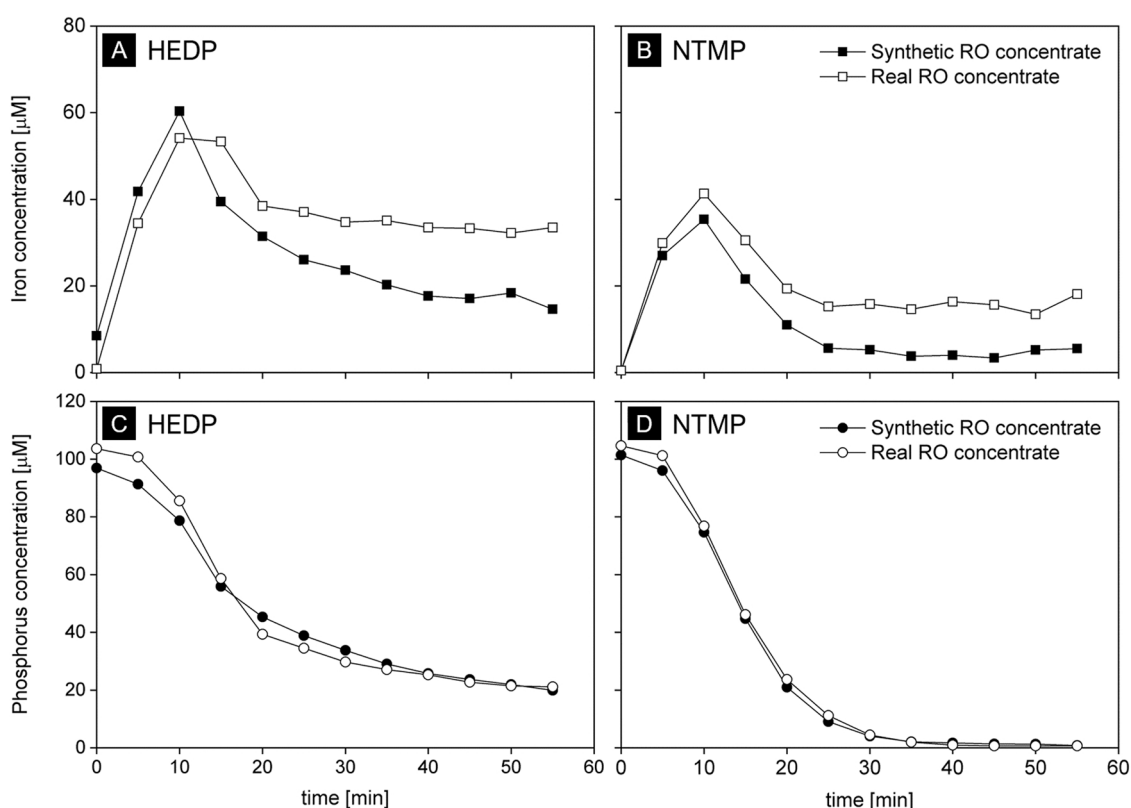
Fig. 4. : Iron and phosphorus concentrations as a function of time in the presence of (A), (C) HEDP, and (B) (D) NTMP phosphonates. Matrix: SROC and RROC, IS: 41.27 and 51.55 mM (Pitzer model), respectively. Initial Phosphorus concentration: 100 µM. Applied current density: 70 A·m^{-2}. The pH of SROC and RROC remained constant throughout the experiments at 7.82 and 7.86, respectively.

Regarding the phosphorus removal, Fig. 4**C** and Fig. 4**D** show that 80% of the HEDP was removed from SROC and RROC when 70 A·m^{-2} current density was applied for one hour. On the contrary, only 20 min were necessary to remove almost 100% of the NTMP. This means that mono and multivalent ions (K^+, Na^+, Mg^{2+}, SO_4^{2-}, NO_3^-) or silica do not interfere or compete with the phosphonates for being adsorbed. These results also show that synthetic concentrate is appropriate in future studies on phosphonate removal from concentrates by electro-coagulation.

When testing EC with NaCl solution as the electrolyte, the dissolved iron reached a higher maximum concentration than in other experiments, as shown in Fig. 5**A**. This is due to the high chloride concentration, which will be further discussed later [49]. The iron concentration profile also indicates relatively faster iron dissolution than hydroxide precipitation. With the $CaCl_2$-based electrolyte, in Fig. 5**B**, the iron dissolution and precipitation speeds were closer to each other, leaving a residual iron concentration of less than 50 µM. Fig. 5**C** shows almost no iron dissolution with the $NaHCO_3$ electrolyte. Al-Raad et al. [50]
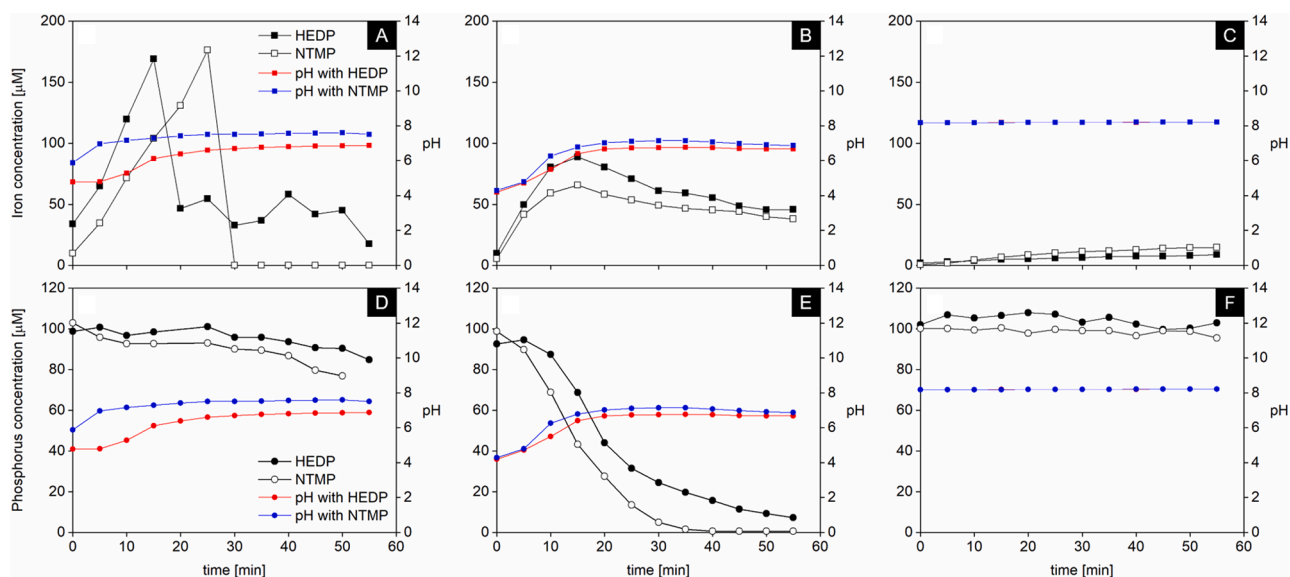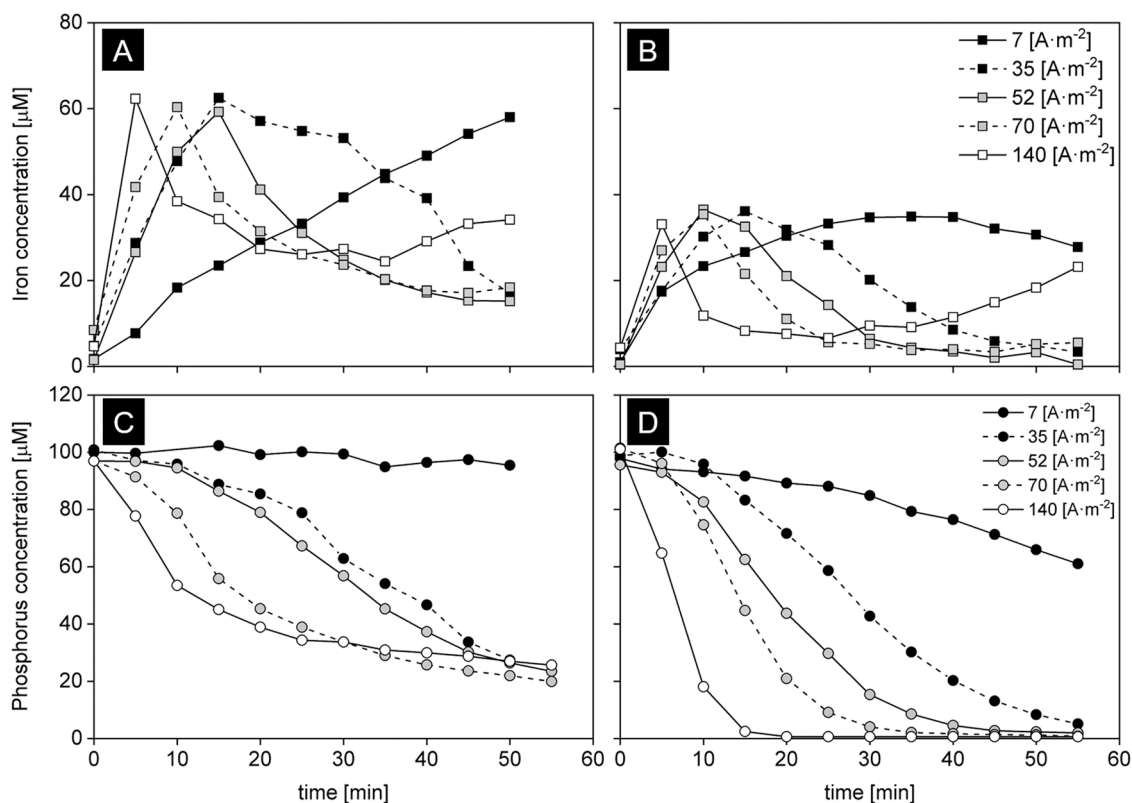
Fig. 5. : pH and iron and phosphorus concentration profiles as function of time in different electrolytes (A), (D) NaCl (41 mM), (B), (E) CaCl$_2$ (14 mM), and (C), (F) NaHCO$_3$ (41 mM). Phosphorus initial concentration: 100 μM. Applied current density: 70 A·m^{-2}. IS: 41 mM.

showed that oxygen could be produced at the anode, (2), at alkaline pH and high enough potential. The oxygen production enhances the formation of a double passivation layer, which protects the anode from being dissolved [51], hence no phosphorus removal was found in this case, Fig. 5F.

$$2H_2O \rightarrow O_2 + 4H^+ + 4e^- \qquad (2)$$

Fig. 5D shows that only about 20% of the initial phosphorus was

removed when the electrolyte only contained NaCl after 50 min. This result is interesting since the iron reached the highest concentration in the solution and the flocs precipitation was abundant in this experiment. On the other hand, the phosphorus removal was comparable to that with SROC and RROC when using CaCl$_2$-based electrolyte. Even the HEDP removal was improved with the CaCl$_2$ (see Fig. 5E). This suggests that not only dissolved iron is determinant for effective phosphorus removal. Calcium plays a double role by stabilizing the iron precipitates and

Fig. 6. : Variation of iron and phosphorus concentrations in SROC along time with HEDP (A) and (C), and NTMP (B) and (D) phosphonates. CaCl$_2$ concentration: 9 mM, NaHCO$_3$ concentration: 14 mM. Initial phosphorus concentration 100 μM. Applied current densities: 7, 35, 52, 70, and 140 A·m^{-2}, IS: 41.27 mM (Pitzer model), initial pH: 7.82.

enhancing the adsorption of the phosphonates on the ferrous surfaces. The formation of the complex Fe-Ca-P during electrocoagulation with iron electrodes promotes the attractive electrostatic interactions between floc clusters close to each other. So, calcium would facilitate the coalescence of the flocs, as recently reported by Mishima et al. [52]. Nowak [11] and Boels [15] also proved a better performance of an iron-based adsorbent for NTMP phosphonate adsorption. Similar results were obtained by Liao et al. [53] when treating cooling tower blowdown (CTB) waters by electrocoagulation to remove silica, calcium, and magnesium. They observed faster calcium and phosphonate removal when both were present in the CTB. This phenomenon can be explained by the calcium being weakly physisorbed on the deprotonated sites of the surface. This first adsorption would increase the number of positive charges, enhancing the subsequent adsorption of the phosphonates.

3.2. Effect of the applied current density

EC experiments comparing RROC and SROC showed similar outcomes regarding phosphorus removal in Fig. 4C and Fig. 4D. Therefore, SROC was chosen to further study the effect of the current density on the iron and phosphorus concentration profiles. For higher current densities (52 – 140 A·m^{-2}), the iron concentration reached a maximum and subsequently decreased, as shown in the previous section. When using HEDP, the dissolution kinetics, dn/dt, during the experiment's first seven to ten minutes were faster than with NTMP (Fig. 6A and Fig. 6B). Furthermore, the remaining iron concentration at the last stages of the experiments was also higher for HEDP than for NTMP. Combined, these two phenomena suggest that HEDP could have better dispersant activity than NTMP in these conditions. Dispersant and coagulant properties are counter effects, and both phosphonates have been previously reported as anionic dispersant agents [4]. The HEDP has slightly better dispersant properties than NTMP [54], keeping the iron in solution for longer times, which explains higher concentrations of iron than with NTMP. At lower current densities (7–35 A·m^{-2}), iron dissolution and phosphorus adsorption became slower than the rest. For HEDP, applied 7 A·m^{-2} were not enough for the iron to reach the maximum concentration in the one-hour reaction. For NTMP, detecting such maximum and subsequent slow decrease in concentration was possible.

As happens with the iron concentration, two factors influenced the phosphorus removal: the current density and the molecular structure of the two different phosphonates. Fig. 6C and Fig. 6D show faster phosphorus removal kinetics for high current densities. NTMP was removed from the SROC faster and more effectively than the HEDP. Only slightly higher than 80% of the phosphorus in HEDP was adsorbed on the flocs, which was confirmed in the 2 h experiment (Fig. 7B). This result indicates that, for phosphonate removal, the stabilization of the flocs plays a more critical role than the total dissolved iron.
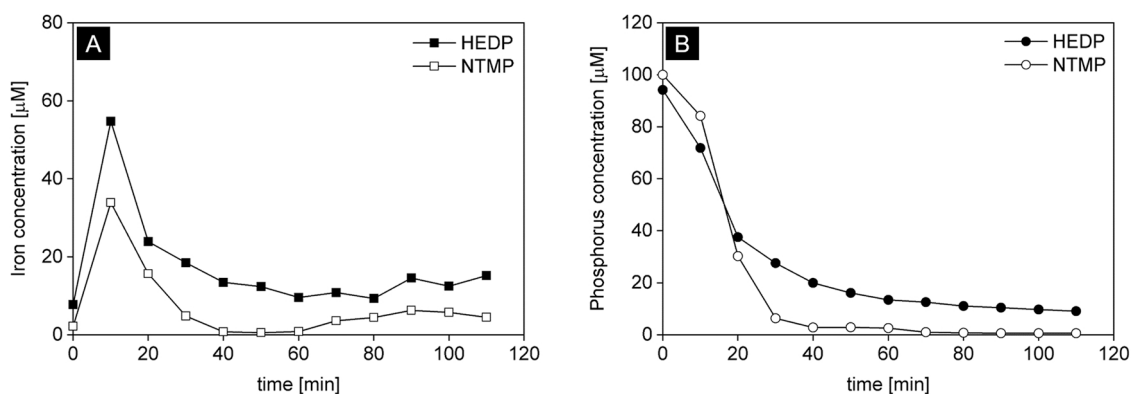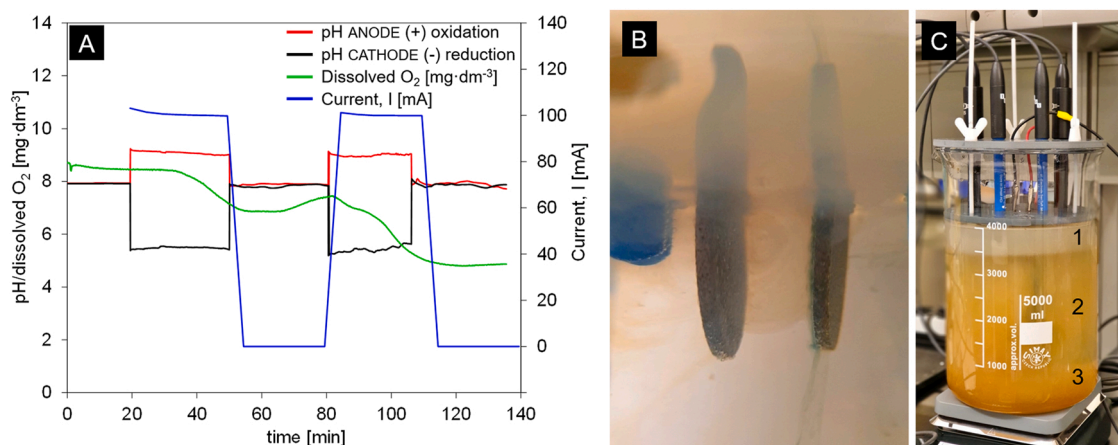
3.3. Experiment without agitation: pH measurements and precipitation

In EC, pH measurements are strongly affected by the electric field between the electrodes and the relative position of the pH probes regarding the cathode and anode [55]. EC experiments without agitation at 70 A·m^{-2} with SROC containing either one of the phosphonates were performed to see what precipitated formed when the electric current was applied. Switching on the power supply changed the initial pH from 7.82 to 9, close to the anode, where the oxidation of the iron occurs (Fig. 8A). Oppositely, the pH went down to 5 near the cathode. When the applied current was put back to zero, the pH recovered its 7.82 initial value. The cycle was repeated, and identical results were obtained. Thus, the pH probe was placed away from the iron electrodes during the rest of the EC experiments, so that changes in the current density would not affect the measurement. On the other hand, the oxygen concentration dropped significantly when applying current, meaning that the oxidation Fe^{2+} → Fe^{3+}, equations (S6) and (S7) in the supporting materials, is also enhanced by the applied potential [56]. The pH in experiments with RROC and SROC remained constant at 7.86 and 7.82, respectively throughout the whole EC process. Contrarily, the pH in the experiments with NaCl evolved from 4.77 to 6.87 with HEDP and from 5.87 to 7.51 with NTMP. Furthermore, the pH of CaCl$_2$ varied from 4.20 to 6.67 with HEDP and from 4.28 to 6.67 with NTMP. The lower initial pH in these cases was due to the presence of the HEDP and NTMP (added in their acidic form) and the absence of the buffering effect of bicarbonate, HCO$_3^-$. Moreover, the dissolved chloride in the electrolyte oxidizes at the anode following the reactions (3) to (5) [27,35], which also contributes to keeping the acidic conditions at the beginning of the experiment.

$$2Cl^- \rightarrow Cl_{2(aq)} + 2e^- \tag{3}$$

$$Cl_{2(aq)} + H_2O \rightarrow HClO + Cl^- + H^+ \tag{4}$$

$$HClO \leftrightarrow ClO^- + H^+ \tag{5}$$

The protonic concentration was eventually neutralized by reactions (S3) and (S4) in the supporting materials, increasing the pH to 7 at the end of the experiments. However, the pH of the solution containing only NaHCO$_3$ showed a constant 8.2 value throughout the process due to the buffering effect of the bicarbonate anion, HCO$_3$.

One of the objectives of this research is to compare the performance of EC for phosphonate removal from RROC and SROC. The pH of these concentrates is buffered at 7.84 ± 0.02 due to the high bicarbonate, (HCO$_3^-$) concentration, thus, this value was considered a constant in most of the experiments. The pH of the electrolytes NaCl and CaCl$_2$ were left in the acidic range and not adjusted to the buffered pH to maintain the ionic strength like the RROC and SROC, as previously mentioned in

Fig. 7. (A) Iron and (B) phosphorus concentration profiles in synthetic concentrate in a 2-hour electrocoagulation experiment. Electrolyte: SROC, CaCl$_2$ concentration: 9 mM, NaHCO$_3$ concentration: 14 mM. Initial phosphorus concentration: 100 µM. Applied current density: 70 A·m^{-2}, IS: 41.27 mM (Pitzer model), initial pH: 7.82.

Fig. 8. (A) pH measurement and dissolved oxygen strongly depended on the applied current density. (B) Green rust was produced during the electrocoagulation experiments. (C) Electrochemical reactor showing well-defined reaction areas during the electrocoagulation process. The light/pale color on top (1) is due to the calcium carbonate precipitate. In this zone is where the electrodes are placed and the electrochemical reactions occur. (2) The area in the middle shows the flocs aggregates coalescing together. (3) The flocs settle down at the bottom of the reactor. Electrolyte: SROC, $CaCl_2$ concentration: 9 mM, $NaHCO_3$ concentration: 14 mM. Initial phosphorus concentration 100 µM from NTMP. Applied current density: 70 A·m^{-2}, IS: 41.27 mM, initial pH: 7.82.

previous sections.

The experiments without agitation also showed a green precipitate coming off the anode (Fig. 8**B**). Such precipitate consists of layered green rust, mainly iron (II) hydroxides with some Fe^{3+} interspersed in the lattice. The charge is compensated by Cl^- or CO_3^{2-}, anions inserted in the structure [57]. During experiments without agitation, three zones eventually were distinguished in the reactor. The top layer (Figs. 8C, 1) acquired a light/pale color due mainly to calcium carbonate precipitation. The produced hydroxyls in the cathode, (reaction S4 in the supporting materials), make pH increase locally, which induces the precipitation of calcium carbonate crystals. The crystals remain on top of the reactor due to their low density and the ascending hydrogen flow. The area in the middle (Figs. 8C, 2) shows the coagulation process where flocs coalesce together, and the iron precipitate undergoes oxidation from Fe^{2+} hydroxides to Fe^{3+} oxides. The aggregated flocs grow and settle down at the bottom of the reactor (Fig. 8**C, 3**). This zone at the bottom of the reactor is red brown, which is mainly constituted by iron oxide (III).

3.4. Characterization of the iron oxide/hydroxides flocs and phosphorus recovery

The flocs produced during the experiments with synthetic concentrate showed fast settling rates of the suspended colloidal matter. After 18 h, the remaining supernatant looked completely clear except for some flocs and calcium carbonate crystals on the surface. 30 mL volume of sludge was produced after the electrocoagulation experiments (see Fig. S1 in the supplementary materials), which represented ~0.75 ± 0.05% of the treated concentrate total volume. After drying the flocs, their mass was reduced to less than one gram. This means that the cost of sludge transportation, treatment, and disposal would mean a minimum part of the process costs.

Calculations with the speciation software PHREECQ v3.5.1 were performed to understand the iron fate in the process. These results predicted the precipitation of different iron (II) and (III) compounds from RROC and SROC during the electrocoagulation experiments (see the results in Table S3 and Table S4 in the supporting materials, respectively). According to the calculations, the flocs would be formed mainly by precipitation of magnetite (Fe_3O_4, Fe (II) and Fe (III)) and hematite (Fe_2O_3, Fe (III)), containing a minor amount of maghemite (Fe_2O_3, Fe (III)), goethite (Fe-OOH, Fe (III)), and akaganéite (Fe $(OH)_{2.7}Cl_{0.3}$, Fe (III)). Therefore, the proportion of iron (III) in the sludge would be more significant than the corresponding iron (II). This points

out that iron (II), produced during electro-oxidation, undergoes fast oxidation into iron (III) according to equations (S6) and (S7) in the supporting materials. The precipitation of crystalline magnetite and hematite and, to a lesser extent, other amorphous iron (oxy)hydroxides have been found in electro-coagulation processes for heavy metals and arsenic removal [58,59]. According to the color of the precipitate (Fig. 8**C**) and the result from the simulations with the PHREECQ v3.5.1 software, the presence of akaganéite and goethite during the EC can be confirmed [60]. Magnetite was also noticed on the agitation bar, under a precipitate protection layer (see Fig. S3 in the supporting materials). Once the flocs sample were collected and filtered, even before the drying step, they dehydrated and transformed into a more thermodynamically stable hematite iron oxide [61] as confirmed by Raman Spectroscopy. Goethite and akaganéite have been confirmed already as good iron-based adsorbents for phosphonates [12,15], which explains the good performance of EC in this case.

The examination of the dry flocs in the scanning electronic microscope, SEM (Fig. 9), showed a homogeneous microporous structure like those described by Kobya et al. [62] under the same experimental conditions. In their work, they confirmed the presence of hydroxyl (–OH) and metal-oxygen-phosphorus (Me-O-P) groups by Fourier transform Infrared Spectroscopy (FTIR), at frequencies 3000–3500 and 1300 cm^{-1} respectively. Back to this work, calcium carbonate (cubic calcite) was found as well-formed crystals (Fig. 9**D** and Fig. 9**F**) and also with imperfections (Fig. 9**C**) showing the integration of the phosphonates in the crystalline lattice. The obtained Raman spectra ($l_0 = $ 532 nm, 5 mW) of our dry flocs (Fig. 10**B** and Fig. 10**C**) showed the characteristic peaks of hematite at 220, 280, 386, 490, 590, and 1282 nm, as compared with other iron oxides and (hydro)oxides in Table 3 [63,64]. As mentioned before, the pics in the low range of the Raman shift could also indicate small residual crystals of goethite, akaganéite, and magnetite. The applied positive potential between the electrodes (5.88 V with HEDP and 10.4 V with NTMP) and the pH of the electrolyte (7.82) both place the system within the iron (III) oxide area in the Pourbaix diagram for iron [65]. Therefore, the presence of iron (II) oxides or hydroxides was negligible, confirming magnetite, goethite, akaganéite, and finally hematite as the primary iron (III) compounds in the flocs.

SEM micrographs (Fig. 9**C**) and Raman spectroscopy (Fig. 11) also confirmed the presence of calcium carbonate crystals, consisting of cubic calcite and round aragonite. Some calcite crystals showed deep and superficial imperfections due to the integration of the phosphonates in the crystalline lattice (Fig. 9**C**). No evidence of phosphate crystals was
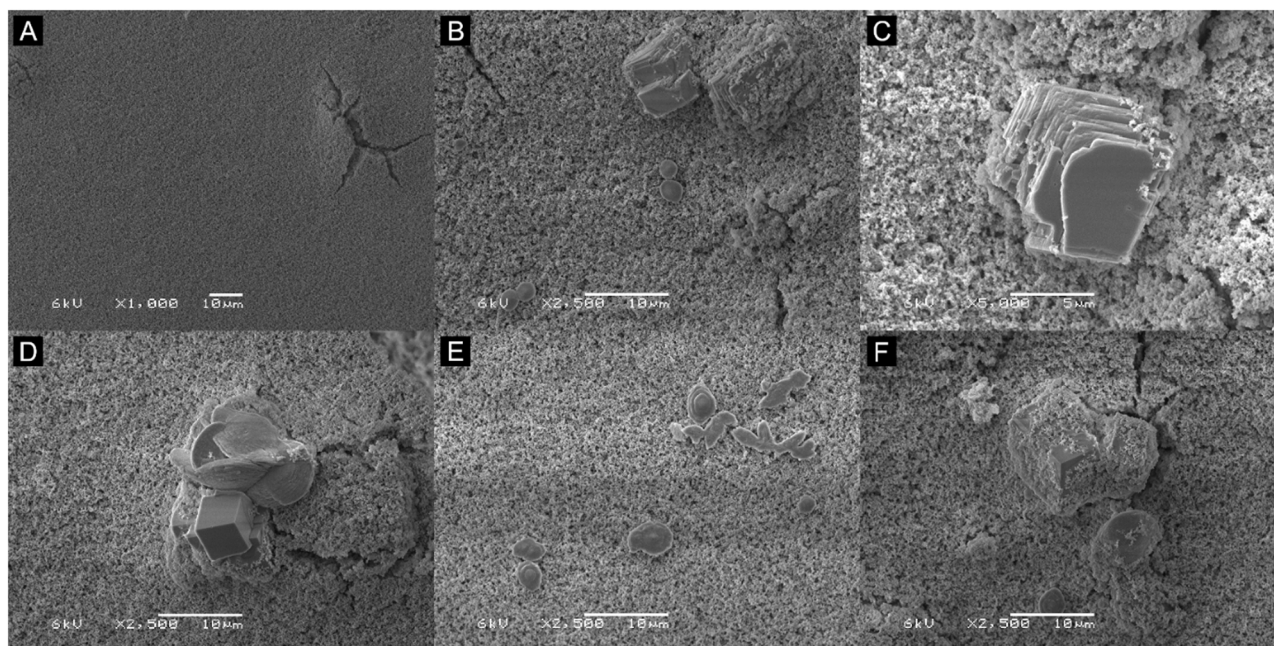
Fig. 9. : SEM images of the dried flocs from electro-coagulation experiments with SROC containing (A), (B), and (C) HEDP and (D), (E), and (F) NTMP. Applied current density: 70 A·m^{-2}, Initial phosphorus concentration: 100 μM.

found in this analysis, as they all can be compared in Table 4 [66]. When analyzing the flocs and crystals, an intensity peak was found at a frequency of 490 cm^{-1}. This vibration is due to the bending motion of the P – O bond, pointing out the presence of free phosphate groups [67]. Phosphonates can be degraded into phosphates by the action of the applied potential [21,40]. Therefore, the presence of P – O groups is due to those in the phosphonate molecules and the phosphates produced from the phosphonate degradation, both adsorbed onto the surface of the flocs and identified by Raman spectroscopy. The performance of EC with iron electrodes has been proven successful for phosphate removal [38], therefore, there is expected competence between phosphates and phosphonates for the adsorption on active sites. Even when comparing such competence is not the objective of this work, further research is needed to elucidate the extent of phosphonate hydrolysis into (ortho) phosphate and will be conducted in future investigations.

Lakshmi Kruthika et al. [31] found CaCl$_2$ scaling on the aluminum electrodes during the EC stage to reduce the total organic carbon (TOC) content in wastewater from a gelatin production plant. In their case, the precipitate affected the performance of the electrodes, so they added carbonate, HCO$_3$, to force the calcium carbonate, CaCO$_3$, precipitation before the EC stage. Our study found no precipitate on the electrodes after applying the electrical potential (see Fig. S3 in the supporting materials) and the EC performance was not affected by the CaCO$_3$ precipitation regarding the phosphonate removal.

Boels et al. [15] used alkaline washing to regenerate granular ferric hydroxide adsorbent (akaganéite, hematite and ferrihydrite [15,73]) once it was saturated with NTMP phosphonate. In this research, we performed preliminary attempts, following the same procedure, to desorb the NTMP and HEDP phosphonates from the sludge produced with SROC. As a result, 100% of the phosphorus was recovered from the NTMP in 2 h, while approximately 63% was recovered from the HEDP after a few days (see Fig. S6A and Fig. S6B in the supporting materials). Therefore, EC is well-suitable for the NTMP since the phosphorus can be adsorbed and desorbed quickly in the complete process. The reason for such a difference is not known yet, hence, the desorption procedure needs further investigation as the presence of calcium carbonate may play an important role in phosphonate recovery. An additional washing step with an acidic solution would dissolve the precipitate, thus accelerating the process [73]. These experimental results can shed new light

and offer new possibilities for the use of recovered phosphorus over a broad range of applications.

The results from the EDS analysis of the precipitated flocs are shown in Fig. S4 and Table S6 for HEDP and Fig. S45 and Table S8 for NTMP in the supporting materials. The EDS spectra revealed the prominent presence of carbon and oxygen. The minor precipitation of carbonates predicted by PHREECQ 3.5.1 calculations cannot explain the high proportion of these two elements on the surface. Thus, the main contribution must come from the polymeric filter itself. The presence of gold can be explained by the coating of the sample previously placed in the electron microscope. As a constituent part of the surface, a small amount of chloride was detected, indicating the potential formation of akaganéite as predicted by the PHREECQ 3.5.1 calculations [74], since no other precipitate containing chloride was expected. The relative atomic abundance of elements differed in terms of P/Fe and Ca/Fe ratios depending on the phosphonates in solution. P/Fe and Ca/Fe for HEDP were 0.25 and 0.5, respectively, while 0.6 and 1 for NTMP. The flocs with NTMP presented more calcium and phosphorus at the surface. These ratios for HEDP suggest the formation of mononuclear mono-dentate between the iron and phosphorus atoms. Thus, the logical disposition for the NTMP, on the other hand, would be mononuclear mono-dentate. In both cases, the calcium would be facilitating the link between the surface and the phosphonate groups. The P/Ca ratios measured by EDS were 0.44 and 0.54 for the HEDP and NTMP, respectively. These ratios indicate the higher potential of the NTMP to complex calcium, which would further enhance its higher adsorption rate on the iron oxide surface. Density Functional Theory (DFT), simulations showed that the formation of bidentate complexes is energetically more favorable than mono-dentate complexes in chemisorption of NTMP on iron hydroxide surfaces [75]. Even when these simulations help understand intermolecular interactions between the NTMP and the iron on the surface, some other factors must be considered. Steric hindrance, electrostatic interaction between chemisorbed and dissolved phosphonates molecules, or underestimation of energy barriers for transition states [76] should be considered in future investigations.

3.5. Economic assessment

The coulombic efficiencies (*CE*) at 70 A·m^{-2} current density, used as
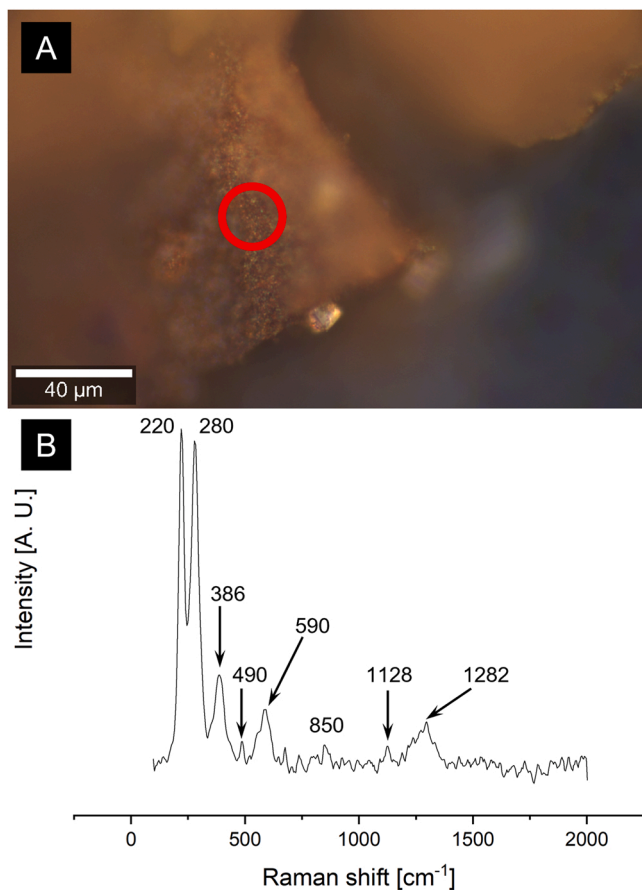
Fig. 10. (A) Sludge micrograph. The red circle corresponds to the area where the laser for the Raman analysis was applied. (B) Raman spectra (baseline subtracted) were acquired from the sludge (λ_0 = 532 nm, 5 mW). Filtered sludge from synthetic RO membrane concentrate containing NTMP at the end of the experiments. Initial phosphorus concentration: 100 μM, applied current density: 70 A·m^{-2}. A similar result was obtained under the same experimental conditions for the HEDP phosphonate.

Table 3

Raman spectra for different iron oxides and hydroxides.

Iron oxide/hydroxide	Raman shift [cm^{-1}]	Reference
Magnetite (Fe$_3$O$_4$)	310, 554, 672	[63,64]
Hematite (α-Fe$_2$O$_3$)	229, 249, 295, 414, 500, 615, 1332	[63,64]
Maghemite (γ-Fe$_2$O$_3$)	365, 511, 700	[63]
Goethite (α-FeOOH)	243, 299, 385, 479, 550	[64]
Akaganéite (β-FeOOH)	314, 380, 549, 722	[68]

a reference, were estimated for all the different electrolytes and both phosphonates, as shown in Fig. 12A. All the *CE* were computed by Eq. (6), where n_{exp} and n_F are the moles of iron in solution estimated experimentally and predicted by the Faraday's Law of Electrolysis (7) [77] respectively. In Eq. (7), I is the current intensity [A] applied in a specific time interval, t [s], z is the number of exchanged electrons, 2 [-] (assuming Fe^{2+} is formed), and F is the Faraday constant [96485 C·mol^{-1}].

$$CE = \frac{n_{exp}}{n_F}100 \qquad (6)$$

$$n_F = \frac{It}{zF} \qquad (7)$$

As shown in Fig. 12A, *CE's* higher than 100% were estimated for HEDP in NaCl, CaCl$_2$, and synthetic concentrate. For NTMP, however,
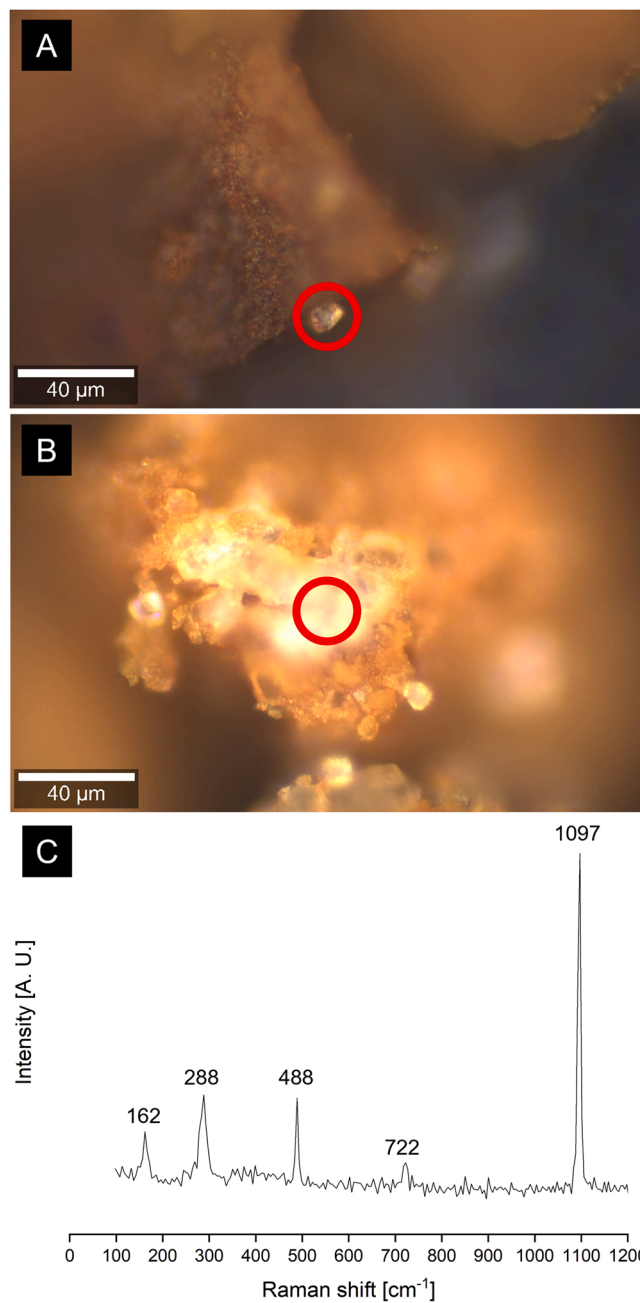

Fig. 11. (A) and (B) Sludge micrograph showing calcium carbonate crystals. The red circles correspond to the area where the Raman spectra were taken. (C) Raman spectra (baseline subtracted) were acquired from the crystals (λ_0 = 532 nm, 5 mW). Filtered sludge from synthetic RO membrane concentrate containing NTMP phosphonate at the end of the experiments. Initial phosphorus concentration 100 μM, applied current density 70 A·m^{-2}. A similar result was obtained under the same experimental conditions for the HEDP phosphonate.

Table 4

Raman spectra for different calcium carbonate polymorphs and free phosphate.

Precipitate	Raman shift [cm^{-1}]	Reference
Calcite (CaCO$_3$)	310, 554, 672	[69]
Vaterite (CaCO$_3$)	229, 249, 295, 414, 500, 615, 1332	[69]
Aragonite (CaCO$_3$)	365, 511, 700	[70]
Free PO$_4^{3-}$	243, 299, 385, 479, 550	[66,67,71,72]
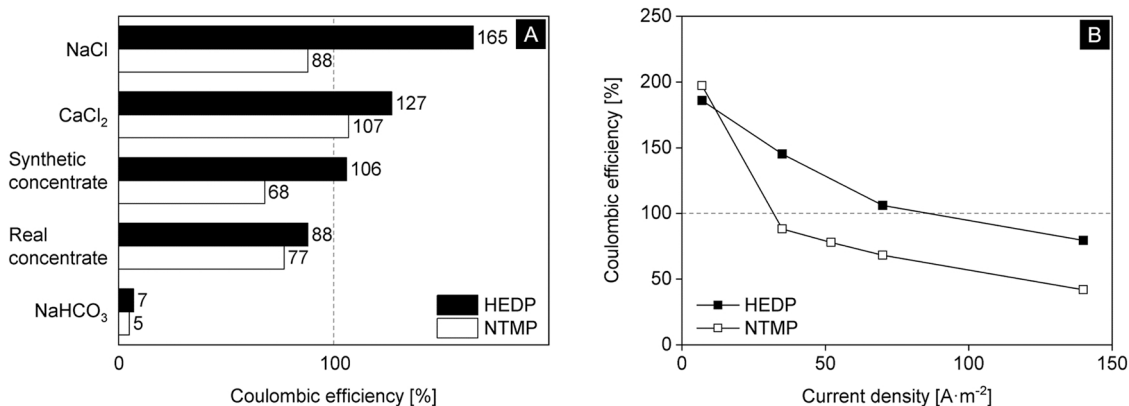
Fig. 12. (A) Coulombic efficiencies in different media for HEDP and NTMP phosphonates. (B) Coulombic efficiencies as a function of the current densities in synthetic concentrate. Current density: 70 A·m^{-2}, $z = 2$ in Faraday's Law.

higher experimental *CE*'s were found only for CaCl$_2$. *CE* higher than 100% is known as superfaradaic efficiency and describes iron concentration in the solution as being higher than that predicted by Faraday's law. This is due to electrochemical and/or chemical reasons. The first one implies the dissolution of the cathode taking place along with hydrogen production. In contrast, the latter includes the chemical oxidation of the anode [78], and both contribute to the total iron concentration in the solution. The chemical oxidation of the anode depends, to a certain extent, on the electrolyte composition. Hydroxyl and chloride ions are active oxidants for iron electrodes [49,79]. Chlorides in particular, follow the reaction sequence (3) to (5), leading to pitting corrosion and subsequent further dissolution of the anode [27,49] (see the effects in Fig. S3 in the supporting materials). In this study, RROC and SROC contained almost two-fold chloride concentration than seawater, which was even higher when using NaCl and CaCl$_2$ as electrolytes. Therefore, in these experimental conditions, the anode undergoes oxidation because of the applied current, enhanced by the additional effect of the high chloride concentration. This agrees with previous research where chloride concentrations below 2 mM already roughly gave 140% *CE*'s [26]. The estimated *CE* showed to be higher at lower current densities, as shown in Fig. 12**B**.

To address the estimation of the costs of the electro-coagulation process only the costs per cubic meter of treated concentrate [€·m^{-3}] and per kilogram of removed phosphorus [€·m^{-3}·kg^{-1}], both inherent to the process itself, will be considered to compute the total cost estimation. That is, the costs of the electrodes and the energy consumption, as shown in Eqs. (8) - (10) [80,81]. Other factors which depend on the size of the water treatment plant or the geographical location, are related to labour, maintenance, cleaning, analytical tasks, transport and disposal of the sludge, etc. [80]. All these mentioned factors are not considered for computing the final cost of EC in this case.

$$\text{Cost estimation} = x_1 C_{electrode} + x_2 C_{energy} \tag{8}$$

$$x_1 = \frac{CE}{100} \frac{ItM_w}{zF\nu} \tag{9}$$

$$x_2 = \frac{EIt}{\nu} \tag{10}$$

$C_{electrode}$ and C_{energy}, are the unitary costs of the iron electrodes [4.5 €·kg^{-1}] and the average price for the electric energy in the European Union were 0.2134 €·(kWh)$^{-1}$ during the second half of 2020 [82]. The parameters x_1 and x_2 are the iron consumed from the anode [kg·m^{-3}] and the electric power applied during the process [kWh·m^{-3}] per cubic meter of treated concentrate, respectively. M_w in Eq. (9) is the molecular mass of iron [kg·mol^{-1}], ν is the volume of treated solution [m^3], and E is the difference of potential measured between the reference electrodes [V]. It is possible to estimate the time at which the operational cost

becomes minimum when the latter is normalized and evaluated per cubic meter of treated concentrate and per kilogram of removed phosphorus, [€·m^{-3}·kg^{-1}]. When treating the SROC with HEDP (Fig. 13**C** and Fig. 13**D**), EC needs to operate, at least 35 or 40 min at 70 and 140 A·m^{-2} respectively to reach the maximum phosphorus concentration allowed by the corresponding Environmental European Legislation [83], which is < 32 μM (1 mg·L^{-1}). Such conditions do not match the minimum operation costs (Fig. 13**A** and Fig. 13**B**), which are at 15 and 10 min. Therefore, 35 min and 70 A·m^{-2} will be the conditions chosen to compute the final operational costs for the HEDP. In the case of NTMP, both 70 and 140 A·m^{-2} showed minimum costs at 20 and 10 min, respectively. In both cases, the phosphorus concentration was below 32 μM; however, operating at 140 A·m^{-2} gave slightly less cost than using at 70 A·m^{-2} for 20 min plus the operational time is reduced in half, from 20 to 10 min. Therefore, those will be the conditions chosen to compute the final operational cost for the NTMP. All the mentioned operating conditions for calculations are summarized in Table 5. Moreover, the minimum costs for all the tested current densities are shown in Fig. S7 in the supporting materials.

The estimated costs were 1.10 €·m^{-3} with HEDP and 0.03 €·m^{-3} with NTMP. These figures agree with cost assessments made by others, using the same methodology, for phosphate removal by electro-coagulation. For example, Lacasa et al. [62] estimated between 0.17 and 1.13 €·m^{-3} for phosphate removal with iron electrodes and initial phosphate concentrations of 0.1 mM. Nguyen et al. [84] optimized the energy consumption per cubic meter of treated concentrate (the equivalent value of x_2 in this study) for phosphate removal with iron electrodes of 0.25 kWh·m^{-3}. Kuokkanen et al. [43] estimated operation costs in phosphate-containing synthetic and real wastewater in the range of 0.17 and 2.11 €·m^{-3}. In this research, the normalized costs per cubic meter of treated concentrate and per kilogram of removed phosphorus are 130.72 and 78.37 €·m^{-3} kg^{-1} for HEDP and NTMP, respectively.

4. Conclusions

Electrocoagulation (EC) technique with pure iron electrodes was successfully tested to remove phosphonates HEDP and NTMP from both real (RROC) and synthetic (SROC) membrane concentrates. Identical results obtained from both concentrates indicate that other anions and compounds in the solution (HCO$_3^-$, SO$_4^-$, NO$_3^-$, silica) did not influence the phosphonate removal by EC. Differences in intrinsic properties of the HEDP and NTMP as complexing agents and surfactants resulted in the total and partial (80%) removal of the NTMP and HEDP, respectively from SROC and RROC. Therefore, depending on the phosphonate in the concentrate, the experimental conditions must be carefully evaluated when choosing EC for phosphonate removal in future works. In this way, more research is needed regarding the applicability of EC to remove
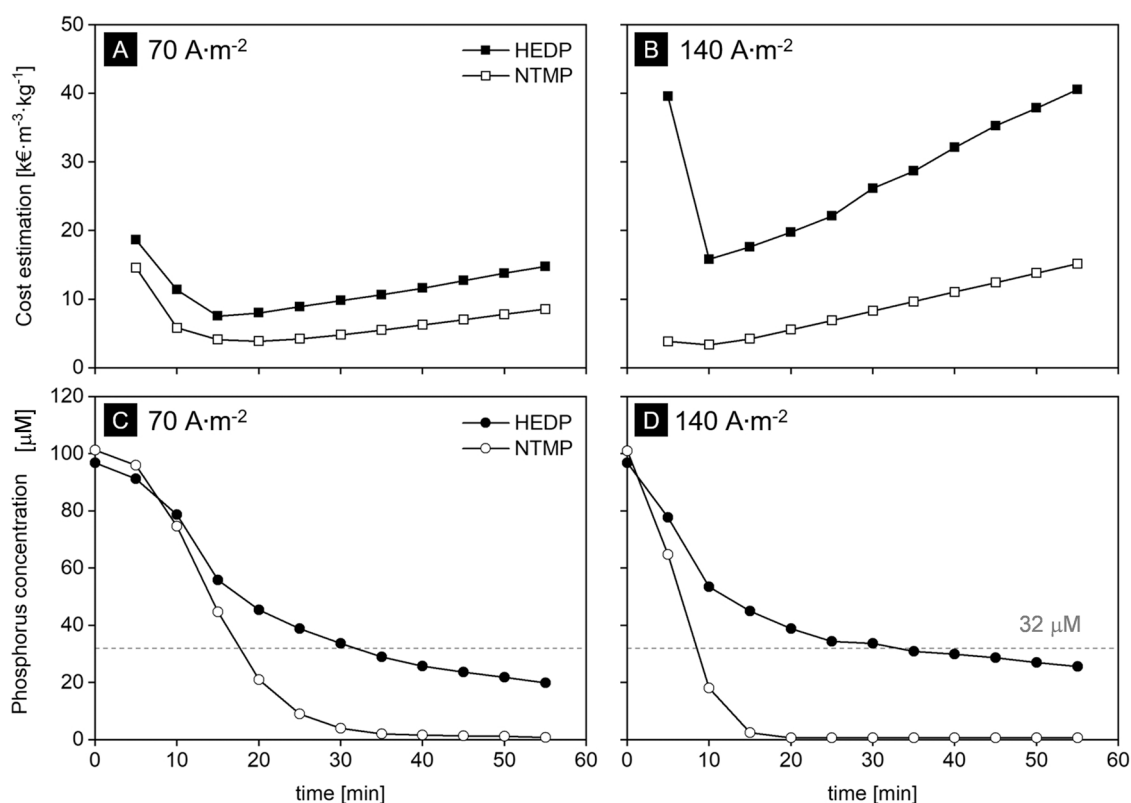
Fig. 13. : Minimum costs estimation per cubic meter of treated synthetic concentrate and per kilogram of removed phosphorus as a function of the experimental time at (A) 70 A·m^{-2} and (B) 140 A·m^{-2} current densities. Phosphorus removal as a function of the testing time at (C) 70 A·m^{-2} and (D) 140 A·m^{-2} current densities. Electrolyte: SROC. The limit of 32 μM (1 mg·L^{-1}) marks the maximum phosphorus concentration in natural waters established by the European Commission [83].

Table 5
Set conditions for cost estimation.

Phosphonate	Current density [A·m^{-2}]	Time [min]	E [V]	x_1, Eq. (9) [kg·m^{-3}]	x_2, Eq. (10) [kWh·m^{-3}]
HEDP	70	35	5.88	0.016	0.090
NTMP	140	10	10.4	0.004	0.090

other phosphonates. Experiments with other electrolytes, NaCl, CaCl$_2$, and NaHCO$_3$ revealed that coulombic efficiencies higher than 100% can be obtained due to anodic oxidation enhanced by the chloride. Furthermore, calcium can determine the effectiveness of EC since its presence improves the flocculation process, and its absence may lead to low phosphonate removal. Calcium carbonate precipitation also contributed to phosphonate removal enhancing the adsorbing properties of the sludge. The produced sludge represented less than 1% of the total treated concentrate volume, which significantly may reduce costs in its subsequent transportation, treatment, and disposal. The collected sludge was characterized as precipitated hematite, indicating the oxidation from iron (II) to iron (III) during the EC process. The treatment of the precipitated flocs with an alkaline solution proved that it is possible to recover the phosphorus from the NTMP completely after 2 h. However, only 63% of the phosphorus from HEDP was desorbed after a few days under the same conditions. The development of an optimized phosphorus recovery procedure as well as the occurrence and extent of phosphonate hydrolysis must be further investigated. In this way, a convenient strategy can be designed to properly valorize the recovered phosphorus. Finally, the economic assessment estimated the optimal operational conditions for each phosphonate: 35 min at 70 A·m^{-2} and 10 min at 140 A·m^{-2} for HEDP and NTMP, respectively. These conditions were used to compute the final EC operational costs, 1.10 and 0.03

€·m^{-3} of treated concentrate for HEDP and NTMP, respectively. This study recognizes for the first time the EC process as an easy-to-control, economically feasible, and chemical-free process for removing phosphonates from concentrates.

CRediT authorship contribution statement

Victor Manuel Torres Serrano, Conceptualization, Methodology, Formal analysis, Data curation, Writing – original draft, Visualization, **Lordina Ekua Eshun,** Methodology, Formal analysis, Investigation, **Andreia Farinha,** Validation, Writing – review & editing, **Geert-Jan Witkamp,** Validation, Writing – review & editing, **Szilard Bucs,** Validation, Writing – review & editing.

Declaration of Competing Interest

The authors declare that they have no known competing financial interests or personal relationships that could have appeared to influence the work reported in this paper.

Data availability

Data will be made available on request.

Appendix A. Supporting information

Supplementary data associated with this article can be found in the online version at doi:10.1016/j.jece.2022.109031.

References

[1] D.M. Warsinger, J. Swaminathan, E. Guillen-Burrieza, H.A. Arafat, J.H. Lienhard V, Scaling and fouling in membrane distillation for desalination applications: a review, Desalination 356 (2015) 294–313, https://doi.org/10.1016/j.desal.2014.06.031.

[2] A. Matin, F. Rahman, H.Z. Shafi, S.M. Zubair, Scaling of reverse osmosis membranes used in water desalination: phenomena, impact, and control; future directions, Desalination 455 (2019) 135–157, https://doi.org/10.1016/j.desal.2018.12.009.

[3] E. Rott, H. Steinmetz, J.W. Metzger, Organophosphonates: a review on environmental relevance, biodegradability and removal in wastewater treatment plants, Sci. Total Environ. 615 (2018) 1176–1191, https://doi.org/10.1016/j.scitotenv.2017.09.223.

[4] B. Nowack, Environmental chemistry of phosphonates, Water Res. 37 (2003) 2533–2546, https://doi.org/10.1016/S0043-1354(03)00079-4.

[5] T. Istirokhatun, M.N. Dewi, H.I. Ilma, H. Susanto, Separation of antiscalants from reverse osmosis concentrates using nanofiltration, Desalination 429 (2018) 105–110, https://doi.org/10.1016/j.desal.2017.12.018.

[6] K.L. Petersen, A. Paytan, E. Rahav, O. Levy, J. Silverman, O. Barzel, D. Potts, E. Bar-Zeev, Impact of brine and antiscalants on reef-building corals in the Gulf of Aqaba – Potential effects from desalination plants, Water Res. 144 (2018) 183–191, https://doi.org/10.1016/j.watres.2018.07.009.

[7] E.K. Read, M. Ivancic, P. Hanson, B.J. Cade-Menun, K.D. McMahon, Phosphorus speciation in a eutrophic lake by ^{31}P NMR spectroscopy, Water Res. 62 (2014) 229–240, https://doi.org/10.1016/j.watres.2014.06.005.

[8] J. Eke, A. Yusuf, A. Giwa, A. Sodiq, The global status of desalination: an assessment of current desalination technologies, plants and capacity, Desalination 495 (2020), 114633, https://doi.org/10.1016/j.desal.2020.114633.

[9] U. Caldera, C. Breyer, Learning curve for seawater reverse osmosis desalination plants: capital cost trend of the past, present, and future, Water Resour. Res 53 (2017) 10523–10538, https://doi.org/10.1002/2017WR021402.

[10] B. Nowack, Aminopolyphosphonate removal during wastewater treatment, Water Res. 36 (2002) 4636–4642, https://doi.org/10.1016/S0043-1354(02)00196-3.

[11] B. Nowack, A.T. Stone, The influence of metal ions on the adsorption of phosphonates onto goethite, Environ. Sci. Technol. 33 (1999) 3627–3633, https://doi.org/10.1021/es9900860.

[12] B. Nowack, A.T. Stone, Adsorption of phosphonates onto the goethite–water interface, J. Colloid Interface Sci. 214 (1999) 20–30, https://doi.org/10.1006/jcis.1999.6111.

[13] B. Nowack, A.T. Stone, Competitive adsorption of phosphate and phosphonates onto goethite, Water Res 40 (2006) 2201–2209, https://doi.org/10.1016/j.watres.2006.03.018.

[14] L. Boels, T. Tervahauta, G.J. Witkamp, Adsorptive removal of nitrilotris (methylenephosphonic acid) antiscalant from membrane concentrates by iron-coated waste filtration sand, J. Hazard Mater. 182 (2010) 855–862, https://doi.org/10.1016/j.jhazmat.2010.06.123.

[15] L. Boels, K.J. Keesman, G.J. Witkamp, Adsorption of phosphonate antiscalant from reverse osmosis membrane concentrate onto granular ferric hydroxide, Environ. Sci. Technol. 46 (2012) 9638–9645, https://doi.org/10.1021/es302186k.

[16] Y. Chen, J.C. Baygents, J. Farrell, Removing phosphonate antiscalants from membrane concentrate solutions using granular ferric hydroxide, J. Water Process Eng. 19 (2017) 18–25, https://doi.org/10.1016/j.jwpe.2017.07.002.

[17] E. Rott, M. Nouri, C. Meyer, R. Minke, M. Schneider, K. Mandel, A. Drenkova-Tuhtan, Removal of phosphonates from synthetic and industrial wastewater with reusable magnetic adsorbent particles, Water Res 145 (2018) 608–617, https://doi.org/10.1016/j.watres.2018.08.067.

[18] E. Rott, R. Minke, H. Steinmetz, Removal of phosphorus from phosphonate-loaded industrial wastewaters via precipitation/flocculation, J. Water Process Eng. 17 (2017) 188–196, https://doi.org/10.1016/j.jwpe.2017.04.008.

[19] S. Sun, S. Wang, Y. Ye, B. Pan, Highly efficient removal of phosphonates from water by a combined Fe(III)/UV/co-precipitation process, Water Res 153 (2019) 21–28, https://doi.org/10.1016/j.watres.2019.01.007.

[20] E. Rott, R. Minke, U. Bali, H. Steinmetz, Removal of phosphonates from industrial wastewater with UV/FeII, Fenton and UV/Fenton treatment, Water Res 122 (2017) 345–354, https://doi.org/10.1016/j.watres.2017.06.009.

[21] Y. Lei, M. Saakes, R.D. van der Weijden, C.J.N. Buisman, Electrochemically mediated calcium phosphate precipitation from phosphonates: Implications on phosphorus recovery from non-orthophosphate, Water Res 169 (2020), 115206, https://doi.org/10.1016/j.watres.2019.115206.

[22] Z. Zhou, W. Qiao, Y. Lin, X. Shen, D. Hu, J. Zhang, L.-M. Jiang, L. Wang, Phosphonate removal from discharged circulating cooling water using iron–carbon micro-electrolysis, Water Sci. Technol. 70 (2014) 524, https://doi.org/10.2166/wst.2014.248.

[23] A. Akyol, Treatment of paint manufacturing wastewater by electrocoagulation, Desalination 285 (2012) 91–99, https://doi.org/10.1016/j.desal.2011.09.039.

[24] P. Cañizares, C. Jiménez, F. Martínez, C. Sáez, M.A. Rodrigo, Study of the electrocoagulation process using aluminum and iron electrodes, Ind. Eng. Chem. Res 46 (2007) 6189–6195, https://doi.org/10.1021/ie070059f.

[25] H.A. Moreno-Casillas, D.L. Cocke, J.A.G. Gomes, P. Morkovsky, J.R. Parga, E. Peterson, Electrocoagulation mechanism for COD removal, Sep Purif. Technol. 56 (2007) 204–211, https://doi.org/10.1016/j.seppur.2007.01.031.

[26] M. ben Sasson, W. Calmano, A. Adin, Iron-oxidation processes in an electroflocculation (electrocoagulation) cell, J. Hazard Mater. 171 (2009) 704–709, https://doi.org/10.1016/j.jhazmat.2009.06.057.

[27] S. Garcia-Segura, M.M.S.G. Eiband, J.V. de Melo, C.A. Martínez-Huitle, Electrocoagulation and advanced electrocoagulation processes: A general review about the fundamentals, emerging applications and its association with other technologies, J. Electroanal. Chem. 801 (2017) 267–299, https://doi.org/10.1016/j.jelechem.2017.07.047.

[28] V.M. García-Orozco, I. Linares-Hernández, R. Natividad, P. Balderas-Hernández, C. Alanis-Ramírez, C.E. Barrera-Díaz, G. Roa-Morales, Solar-photovoltaic electrocoagulation of wastewater from a chocolate manufacturing industry: anodic material effect (aluminium, copper and zinc) and life cycle assessment, J. Environ. Chem. Eng. 10 (2022), 107969, https://doi.org/10.1016/j.jece.2022.107969.

[29] A. Akhtar, Z. Aslam, A. Asghar, M.M. Bello, A.A.A. Raman, Electrocoagulation of congo red dye-containing wastewater: optimization of operational parameters and process mechanism, J. Environ. Chem. Eng. 8 (2020), 104055, https://doi.org/10.1016/j.jece.2020.104055.

[30] M. Elazzouzi, Kh Haboubi, M.S. Elyoubi, Electrocoagulation flocculation as a low-cost process for pollutants removal from urban wastewater, Chem. Eng. Res. Des. 117 (2017) 614–626, https://doi.org/10.1016/j.cherd.2016.11.011.

[31] N. Lakshmi Kruthika, S. Karthika, G. Bhaskar Raju, S. Prabhakar, Efficacy of electrocoagulation and electrooxidation for the purification of wastewater generated from gelatin production plant, J. Environ. Chem. Eng. 1 (2013) 183–188, https://doi.org/10.1016/j.jece.2013.04.017.

[32] J. Ano, B.G. Henri Briton, K.E. Kouassi, K. Adouby, Nitrate removal by electrocoagulation process using experimental design methodology: A techno-economic optimization, J. Environ. Chem. Eng. 8 (2020), 104292, https://doi.org/10.1016/j.jece.2020.104292.

[33] M. Ghazouani, L. Bousselmi, H. Akrout, Combined electrocoagulation and electrochemical treatment on BDD electrodes for simultaneous removal of nitrates and phosphates, J. Environ. Chem. Eng. 8 (2020), 104509, https://doi.org/10.1016/j.jece.2020.104509.

[34] T. Banerji, S. Chaudhari, Arsenic removal from drinking water by electrocoagulation using iron electrodes- an understanding of the process parameters, J. Environ. Chem. Eng. 4 (2016) 3990–4000, https://doi.org/10.1016/j.jece.2016.09.007.

[35] M.S. Oncel, A. Muhcu, E. Demirbas, M. Kobya, A comparative study of chemical precipitation and electrocoagulation for treatment of coal acid drainage wastewater, J. Environ. Chem. Eng. 1 (2013) 989–995, https://doi.org/10.1016/j.jece.2013.08.008.

[36] N. Daneshvar, A. Oladegaragoze, N. Djafarzadeh, Decolorization of basic dye solutions by electrocoagulation: an investigation of the effect of operational parameters, J. Hazard Mater. 129 (2006) 116–122, https://doi.org/10.1016/j.jhazmat.2005.08.033.

[37] J.N. Hakizimana, B. Gourich, M. Chafi, Y. Stiriba, C. Vial, P. Drogui, J. Naja, Electrocoagulation process in water treatment: a review of electrocoagulation modeling approaches, Desalination 404 (2017) 1–21, https://doi.org/10.1016/j.desal.2016.10.011.

[38] T.R. Devlin, M.S. Kowalski, E. Pagaduan, X. Zhang, V. Wei, J.A. Oleszkiewicz, Electrocoagulation of wastewater using aluminum, iron, and magnesium electrodes, J. Hazard Mater. 368 (2019) 862–868, https://doi.org/10.1016/j.jhazmat.2018.10.017.

[39] K.S. Hashim, R. al Khaddar, N. Jasim, A. Shaw, D. Phipps, P. Kot, M.O. Pedrola, A. W. Alattabi, M. Abdulredha, R. Alawsh, Electrocoagulation as a green technology for phosphate removal from river water, Sep Purif. Technol. 210 (2019) 135–144, https://doi.org/10.1016/j.seppur.2018.07.056.

[40] X. Zhang, Y. Wang, M. Feng, G.E. Yuan, Comparison of electrocoagulation and chemical coagulation in removal of phosphonate chelators from water, Water Sci. Technol. 85 (2022) 2015–2026, https://doi.org/10.2166/wst.2022.108.

[41] J.W. Mullin. Crystallization, 4th ed..,, Butterworth-Heinemann,, 2001.

[42] D.L. Parkhurst, C.A.J. Appelo, et al., User's guide to PHREEQC (Version 2): A computer program for speciation, batch-reaction, one-dimensional transport, and inverse geochemical calculations, Water-Resour. Investig. Rep. 99 (1999) 312.

[43] V. Kuokkanen, T. Kuokkanen, J. Rämö, U. Lassi, J. Roininen, Removal of phosphate from wastewaters for further utilization using electrocoagulation with hybrid electrodes – Techno-economic studies, J. Water Process Eng. 8 (2015) e50–e57, https://doi.org/10.1016/j.jwpe.2014.11.008.

[44] Y. Tian, W. He, D. Liang, W. Yang, B.E. Logan, N. Ren, Effective phosphate removal for advanced water treatment using low energy, migration electric–field assisted electrocoagulation, Water Res 138 (2018) 129–136, https://doi.org/10.1016/j.watres.2018.03.037.

[45] Y. Tian, W. He, X. Zhu, W. Yang, N. Ren, B.E. Logan, Improved electrocoagulation reactor for rapid removal of phosphate from wastewater, ACS Sustain Chem. Eng. 5 (2017) 67–71, https://doi.org/10.1021/acssuschemeng.6b01613.

[46] P.I. Omwene, M. Kobya, Treatment of domestic wastewater phosphate by electrocoagulation using Fe and Al electrodes: a comparative study, Process Saf. Environ. Prot. 116 (2018) 34–51, https://doi.org/10.1016/j.psep.2018.01.005.

[47] J.L. Fang, Y. Li, X.R. Ye, Z.W. Wang, Q. Liu, Passive films and corrosion protection due to phosphonic acid inhibitors, Corrosion 49 (1993) 6, https://doi.org/10.5006/1.3316048.

[48] Y. Chen, J.C. Baygents, J. Farrell, Evaluating electrocoagulation and chemical coagulation for removing dissolved silica from high efficiency reverse osmosis (HERO) concentrate solutions, J. Water Process Eng. 16 (2017) 50–55, https://doi.org/10.1016/j.jwpe.2016.12.008.

[49] M.G. Arroyo, V. Pérez-Herranz, M.T. Montañés, J. García-Antón, J.L. Guiñón, Effect of pH and chloride concentration on the removal of hexavalent chromium in a batch electrocoagulation reactor, J. Hazard Mater. 169 (2009) 1127–1133, https://doi.org/10.1016/j.jhazmat.2009.04.089.

[50] A.A. Al-Raad, M.M. Hanafiah, Removal of inorganic pollutants using electrocoagulation technology: a review of emerging applications and mechanisms, J. Environ. Manag. 300 (2021), 113696, https://doi.org/10.1016/j.jenvman.2021.113696.

[51] H. DorMohammadi, Q. Pang, P. Murkute, L. Árnadóttir, O. Burkan Isgor, Investigation of iron passivity in highly alkaline media using reactive-force field molecular dynamics, Corros. Sci. 157 (2019) 31–40, https://doi.org/10.1016/j.corsci.2019.05.016.

[52] I. Mishima, M. Hama, Y. Tabata, J. Nakajima, Improvement of phosphorus removal by calcium addition in the iron electrocoagulation process, Water Sci. Technol. 76 (2017) 920–927, https://doi.org/10.2166/wst.2017.256.

[53] Z. Liao, Z. Gu, M.C. Schulz, J.R. Davis, J.C. Baygents, J. Farrell, Treatment of cooling tower blowdown water containing silica, calcium and magnesium by electrocoagulation, Water Sci. Technol. 60 (2009) 2345–2352, https://doi.org/10.2166/wst.2009.675.

[54] Z. Amjad, Investigations on the influence of phosphonates in dispersing iron oxide (rust) by polymeric additives for industrial water applications, Int. J. Corros. Scale Inhib. 3 (2014) 89–100, https://doi.org/10.17675/2305-6894-2014-3-2-089-100.

[55] H.A. Moreno C, D.L. Cocke, J.A.G. Gomes, P. Morkovsky, J.R. Parga, E. Peterson, C. Garcia, Electrochemical Reactions for Electrocoagulation Using Iron Electrodes, in: Ind Eng Chem Res., 48, 2009, pp. 2275–2282, https://doi.org/10.1021/ie8013007.

[56] A. Doggaz, A. Attour, M. Le Page Mostefa, M. Tlili, F. Lapicque, Iron removal from waters by electrocoagulation: Investigations of the various physicochemical phenomena involved, Sep Purif. Technol. 203 (2018) 217–225, https://doi.org/10.1016/j.seppur.2018.04.045.

[57] U. Schwertmann, R.M. Cornell, Green Rusts, in: Iron Oxides in the Laboratory: Preparation and Characterization, 2nd ed.,, Wiley-VCH, 2000.

[58] D.-G. Kim, R.J.S. Palacios, S.-O. Ko, Characterization of sludge generated by electrocoagulation for the removal of heavy metals, Desalin. Water Treat. 52 (2014) 909–919, https://doi.org/10.1080/19443994.2013.826776.

[59] J.A.G. Gomes, P. Daida, M. Kesmez, M. Weir, H. Moreno, J.R. Parga, G. Irwin, H. McWhinney, T. Grady, E. Peterson, D.L. Cocke, Arsenic removal by electrocoagulation using combined Al–Fe electrode system and characterization of products, J. Hazard Mater. 139 (2007) 220–231, https://doi.org/10.1016/j.jhazmat.2005.11.108.

[60] R.M. Cornell, U. Schwertmann, Introduction to iron oxydes, in: The Iron Oxides: Structure, Properties, Reaction, Occurences, and Uses, 2nd ed., Wiley-VCH Verlag GmbH & Co. KGaA, Weinheim, 2003.

[61] R.M. Cornell, U. Schwertmann, Transformation, in: The Iron Oxides: Structure, Properties, Reaction, Occurences, and Uses, 2nd ed.,, Wiley-VCH Verlag GmbH & Co. KGaA, Weinheim, 2003.

[62] M. Kobya, P.I. Omwene, S.M. Sarabi, S. Yildirim, Z. Ukundimana, Phosphorous removal from anaerobically digested municipal sludge centrate by an electrocoagulation reactor using metal (Al, Fe and Al-Fe) scrap anodes, Process Saf. Environ. Prot. 152 (2021) 188–200, https://doi.org/10.1016/j.psep.2021.06.003.

[63] A.M. Jubb, H.C. Allen, Vibrational spectroscopic characterization of hematite, maghemite, and magnetite thin films produced by vapor deposition, ACS Appl. Mater. Interfaces 2 (2010) 2804–2812, https://doi.org/10.1021/am1004943.

[64] D.L.A. de Faria, F.N. Lopes, Heated goethite and natural hematite: can Raman spectroscopy be used to differentiate them? Vib. Spectrosc. 45 (2007) 117–121, https://doi.org/10.1016/j.vibspec.2007.07.003.

[65] L.L. Pesterfield, J.B. Maddox, M.S. Crocker, G.K. Schweitzer, Pourbaix (E–pH-M) diagrams in three dimensions, J. Chem. Educ. 89 (2012) 891–899, https://doi.org/10.1021/ed200423n.

[66] M. Kazanci, P. Fratzl, K. Klaushofer, E.P. Paschalis, Complementary information on in vitro conversion of amorphous (precursor) calcium phosphate to hydroxyapatite from Raman microspectroscopy and wide-angle X-ray scattering, Calcif. Tissue Int 79 (2006) 354–359, https://doi.org/10.1007/s00223-006-0011-9.

[67] J.A. Stammeier, B. Purgstaller, D. Hippler, V. Mavromatis, M. Dietzel, In-situ Raman spectroscopy of amorphous calcium phosphate to crystalline hydroxyapatite transformation, MethodsX 5 (2018) 1241–1250, https://doi.org/10.1016/j.mex.2018.09.015.

[68] S. Réguer, D. Neff, L. Bellot-Gurlet, P. Dillmann, Deterioration of iron archaeological artefacts: micro-Raman investigation on Cl-containing corrosion products, J. Raman Spectrosc. 38 (2007) 389–397, https://doi.org/10.1002/jrs.1659.

[69] F.C. Donnelly, F. Purcell-Milton, V. Framont, O. Cleary, P.W. Dunne, Y.K. Gun'ko, Synthesis of CaCO3 nano- and micro-particles by dry ice carbonation, Chem. Commun. 53 (2017) 6657–6660, https://doi.org/10.1039/C7CC01420A.

[70] J.E. Parker, S.P. Thompson, A.R. Lennie, J. Potter, C.C. Tang, A study of the aragonite-calcite transformation using Raman spectroscopy, synchrotron powder diffraction and scanning electron microscopy, CrystEngComm 12 (2010) 1590–1599, https://doi.org/10.1039/B921487A.

[71] P.N. de Aza, C. Santos, A. Pazo, S. de Aza, R. Cuscó, L. Artús, Vibrational properties of calcium phosphate compounds. 1. Raman Spectrum of β-tricalcium phosphate, Chem. Mater. 9 (1997) 912–915, https://doi.org/10.1021/cm960425d.

[72] P.N. de Aza, F. Guitián, C. Santos, S. de Aza, R. Cuscó, L. Artús, Vibrational properties of calcium phosphate compounds. 2. comparison between hydroxyapatite and β-tricalcium phosphate, Chem. Mater. 9 (1997) 916–922, https://doi.org/10.1021/cm9604266.

[73] P. Suresh Kumar, W.W. Ejerssa, C.C. Wegener, L. Korving, A.I. Dugulan, H. Temmink, M.C.M. van Loosdrecht, G.-J. Witkamp, Understanding and improving the reusability of phosphate adsorbents for wastewater effluent polishing, Water Res 145 (2018) 365–374, https://doi.org/10.1016/j.watres.2018.08.040.

[74] U. Schwertmann, R.M. Cornell, Akaganéite, in: Iron Oxides in the Laboratory: Preparation and Characterization, 2000, pp. 113–119, https://doi.org/10.1002/9783527613229.ch09.

[75] R.J. Martínez, J. Farrell, Understanding Nitrilotris(methylenephosphonic acid) reactions with ferric hydroxide, Chemosphere 175 (2017) 490–496, https://doi.org/10.1016/j.chemosphere.2017.02.015.

[76] A.J. Cohen, P. Mori-Sánchez, W. Yang, Insights into current limitations of density functional theory, 792 LP – 794, Science 321 (2008) (1979), https://doi.org/10.1126/science.1158722.

[77] B. Bhattacharyya, Chapter 2 - Electrochemical Machining: Macro to Micro, in: B.B. T.-E.M. for N. Bhattacharyya MEMS and Nanotechnology (Ed.), Micro and Nano Technologies, William Andrew Publishing, 2015: pp. 25–52. https://doi.org/https://doi.org/10.1016/B978–0-323–32737-4.00002–5.

[78] C.E. Barrera-Díaz, P. Balderas-Hernández, B. Bilyeu, in: C.A. Martínez-Huitle, M.A. Rodrigo, O.B.T. -E.W, W.T. Scialdone (Eds.), - Electrocoagulation: Fundamentals and Prospectives, Butterworth-Heinemann, 2018, pp. 61–76, https://doi.org/10.1016/B978-0-12-813160-2.00003-1.

[79] T. Picard, G. Cathalifaud-Feuillade, M. Mazet, C. Vandensteendam, Cathodic dissolution in the electrocoagulation process using aluminium electrodes, J. Environ. Monit. 2 (2000) 77–80, https://doi.org/10.1039/A908248D.

[80] M. Kobya, E. Demirbas, Evaluations of operating parameters on treatment of can manufacturing wastewater by electrocoagulation, J. Water Process Eng. 8 (2015) 64–74, https://doi.org/10.1016/j.jwpe.2015.09.006.

[81] M. Kobya, H. Hiz, E. Senturk, C. Aydiner, E. Demirbas, Treatment of potato chips manufacturing wastewater by electrocoagulation, Desalination 190 (2006) 201–211, https://doi.org/10.1016/j.desal.2005.10.006.

[82] Eurostat, Electricity price Statistics: Electricity prices (includding taxes) for households costumers, second half 2020, Eurostat Statistics Explained. (2021). https://ec.europa.eu/eurostat/statistics-explained/index.php?title=Electricity_price_statistics (accessed September 23, 2021).

[83] EU Comission, COUNCIL DIRECTIVE of 21 May 1991 concerning urban waste water treatment, 2014. https://eur-lex.europa.eu/legal-content/EN/TXT/PDF/?uri=CELEX:01991L0271–20140101&from=EN.

[84] D.D. Nguyen, H.H. Ngo, W. Guo, T.T. Nguyen, S.W. Chang, A. Jang, Y.S. Yoon, Can electrocoagulation process be an appropriate technology for phosphorus removal from municipal wastewater? Sci. Total Environ. 563–564 (2016) 549–556, https://doi.org/10.1016/j.scitotenv.2016.04.045.